LEE WAVES OVER THE UK : OBSERVATIONS AND MODEL SIMULATION

G.J. Shutts and A.S. Broad
U.K. Meteorological Office
Bracknell, England

Summary : Observations of lee waves from three small field experiments held in mountainous (or hilly) regions of the UK are presented. These form the basis of three case studies using a non-hydrostatic mesoscale model, with realistic terrain height specification and gridpoint spacing of between 1 and 3 Km - dependent on the region of interest. Each of the three model simulations discussed here runs to a quasi-steady state after about four hours and the resulting vertical velocity fields are compared directly with those deduced from radiosonde ascent rate fluctuations and, in one case, aircraft data. The agreement is very encouraging and suggests that stationary orographic lee waves, unlike many small to mesoscale phenomena, are quite predictable. Direct simulation may therefore provide a method for estimating gravity wave drag over complex terrain and a means for refining gravity wave drag parametrization schemes.

1. INTRODUCTION

Research into atmospheric gravity waves has been spurred on in the last decade by the recognition of the important rôle played by wave drag in the global momentum budget. In the mesosphere, gravity wave stress is a dominating dynamical influence whilst in the troposphere and lower stratosphere it plays a secondary rôle in the momentum budget of the zonally-averaged flow. The incorporation of gravity wave drag parametrization schemes into operational forecast and climate models (e.g. Boer et al, 1984; Palmer et al, 1986 and Macfarlane, 1987) has been shown to eliminate much of the systematic westerly wind model bias in middle latitudes of the northern hemisphere and their use is now standard. However, many aspects of these schemes are over-simplified and some completely ignore wave-trapping and assume free upward radiation of wave energy until some condition for wave-breaking is satisfied. The practical motivation to study and observe *trapped* lee wave motion is therefore strong.

In this context, it is important to know whether or not the assumed level of gravity wave activity implied in parametrization schemes is realistic for a wide range of orographic types (e.g. rolling hills or rugged mountainous terrain). Furthermore, the widespread interest in gravity wave drag parametrization may have unfairly directed attention away from the rôle of the boundary layer in complex terrain. The relative size of the net aerodynamic form drag to the gravity wave stress remains unknown. Field experiments continue to play an essential rôle in providing information about these orographically-forced flows and the data collected are being used increasingly to verify direct model simulations of actual cases.

The three case studies described here were drawn from small field experiments held in Wales, Scotland and Cumbria. Radiosonde sondes were released singly in the Scottish experiment; in groups of three in the Welsh experient and in groups of up to five in the Cumbrian field experiment. Rate-of-ascent fluctuations about a fairly constant *still air* value are due mainly to vertical air motion and clearly reveal the presence of gravity wave motion (e.g. Corby, 1957; Kitchen and Shutts, 1990). The radiosonde rate-of-ascent is computed from the pressure tendency using the hydrostatic equation applied to layers about 200 m thick.

A multiple sonde technique has been developed in which up to five sondes can be released in rapid succession (with about three to ten minute time separation) each balloon receiving slightly more Helium gas so that a range of mean ascent rates can be achieved. Ideally this range extends from a minimum of 2 ms^{-1} to a maximum of 5 ms^{-1}, being constrained by the cost of gas and lower burst height at the high end; and the likelihood of the sonde hitting the ground, tree or

building shortly after launch at the low end. The dispersed sonde trajectories in the vertical plane sample different portions of the gravity wave field and can provide information concerning the slope of phase lines (Shutts et al, 1992). In the Cumbrian field experiment we were lucky enough to be able to combine five sonde profiles with aircraft data obtained on four level flight legs : enough data was obtained to subjectively plot a vertical cross-section of vertical velocity.

The bulk of this paper will be concerned with high resolution numerical simulations of stationary lee waves using an adapted version of the British Meteorological Office's operational Mesoscale model (see Golding, 1987). The model, developed originally by Tapp and White (1976), solves the fully compressible, non-hydrostatic equations of motion on a regular Cartesian, Arakawa C grid with vertical velocity held on intermediate levels. A semi-implicit treatment of acoustic modes avoids time step dependence on the speed of sound. Following Carpenter (1979), the vertical coordinate (η) is given by:

$$\eta = z - E(x, y) \tag{1}$$

where $E(x, y)$ is the terrain height and z is the actual height above mean sea-level.

In the three cases to be presented, horizontal gridlengths of between 1 and 3 Km were used with 32 or 43 vertical levels. An upper damping layer was used to minimize reflection from the upper lid. This took the form of a linear increase of horizontal diffusion to some very high value near the model top combined with a Newtonian damping term added to all prognostic equations relaxing fields to their initial state.

The time constant (τ) of this damping term is given by:

$$\tau = \tau_* \left(\exp\left(\frac{z - z_*}{z_d}\right) - 1 \right)^{-1} \tag{2}$$

where z_* is the height of the bottom of the damping layer.

All model integrations were dry (relative humidity set to 1% initially) with surface energy fluxes and radiative transfer switched off for the purpose of these case studies. The model has a $1\frac{1}{2}$ order turbulence closure scheme involving a prognostic equation for turbulent kinetic energy to compute vertical eddy transfer coefficients K_h and K_m for heat and momentum respectively. Essentially these coefficients are the product of the turbulent kinetic energy and an eddy time scale dependent on the squares of the buoyancy frequency and vertical wind shear. In two of the case studies, land roughness lengths (z_0) were chosen to be proportional to terrain height with a peak value 3 m. Otherwise the operational model default value of 0.1 m was used. Over the sea z_0 was set equal to 10^{-4}. Sensitivity studies have shown that on this horizontal scale, the lee wave response is not significantly dependent on z_0 in the range 0.1 to 3 m. On the other hand, the magnitude of the surface shearing stress and drag coefficient is highly dependent on z_0.

The model was initialized with smoothed profiles of wind and temperature and a linear horizontal variation in pressure and temperature, contrived to satisfy the geostrophic and thermal wind equations respectively, was added.

2. WELSH CASE STUDY - 6 OCTOBER 1989

2.1 Observations

An intense lee wave event occurred on the afternoon of October 6 1989 during a field experiment based just outside the village of Caersws in mid-Wales. The Welsh orography is fairly heterogeneous with mountains typically 400 or 500 metres high and with peak values up to 1000 m in Snowdonia, North Wales.

The synoptic situation at midday on Oct. 6 1989 is represented by the mean sea-level pressure chart in Fig. 1. A fairly strong, west to northwesterly airstream, with embedded frontal system covers most of the UK with Wales lying in the warm sector. Figs. 2 (a), (b), (c), and (d) show the temperature, wind speed, wind direction and relative humidity respectively measured by a sonde released at 1358 GMT. The airstream is moist and fairly stable below 3 Km with static

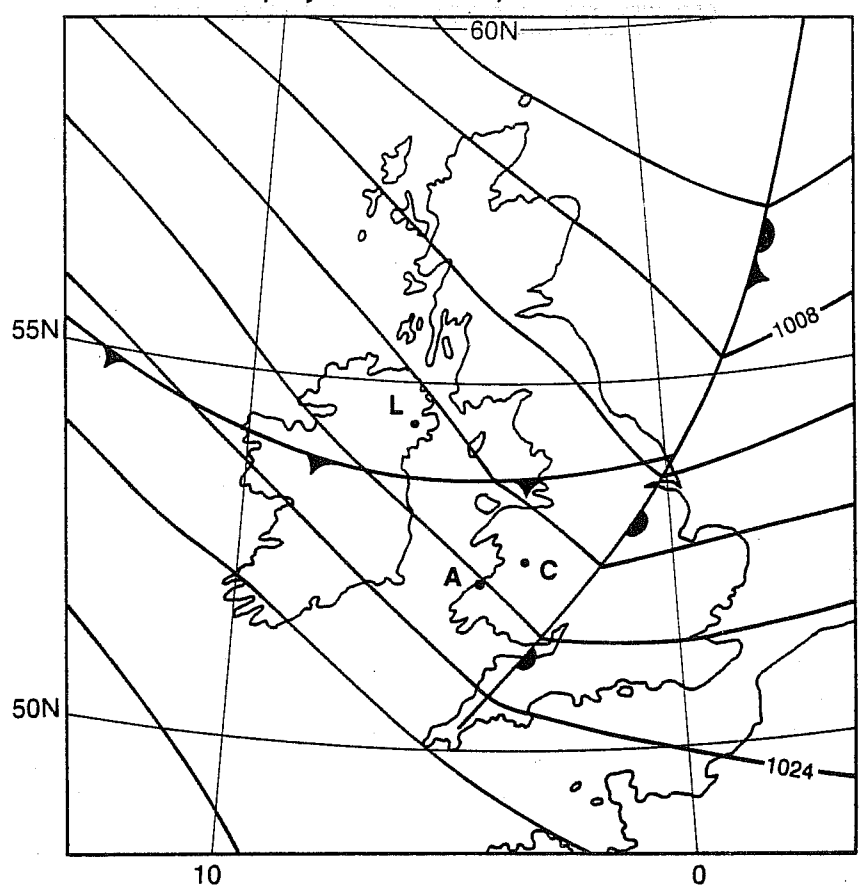

Fig. 1 The synoptic analysis at 12 GMT on 6 October 1989 over the UK. Sea-level pressure is plotted with a 4hPa contour interval. Caersws village and Aberporth are marked by a C and A respectively.

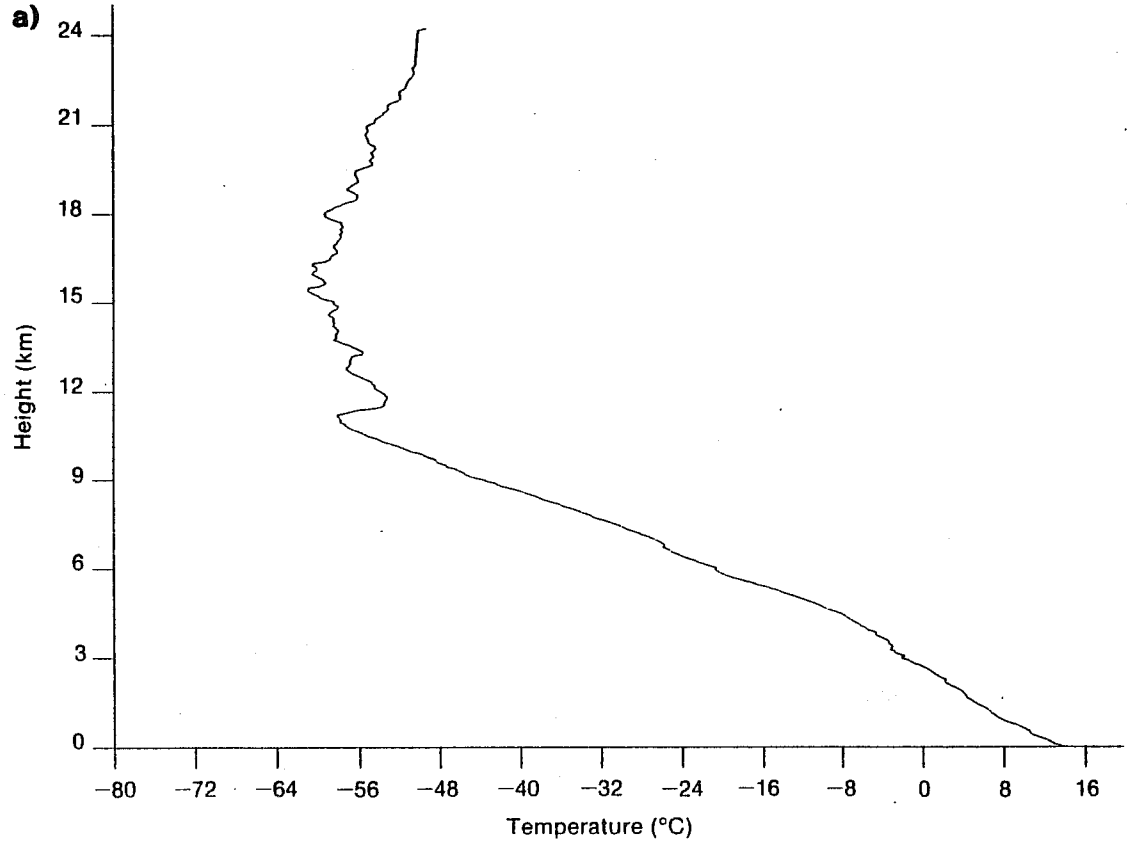

Fig. 2 Vertical profiles of a) temperature, b) wind speed, c) wind direction and relative humidity (solid line) obtained from the sonde released at 1358GMT from Caersws. The dashed line in Fig. 2d) is the realtive humidity obtained from Aberporth ascent made at 1404 GMT.

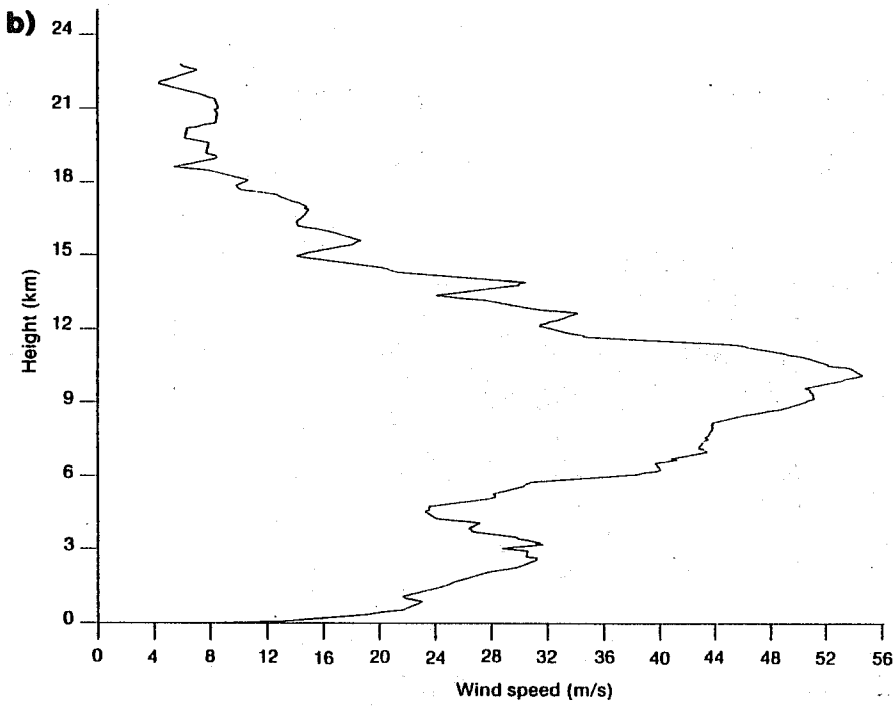

Fig. 2b)

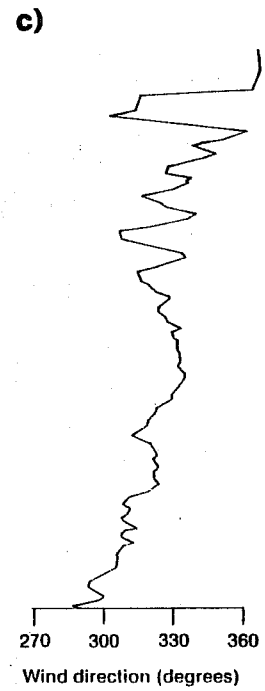

Fig. 2c)

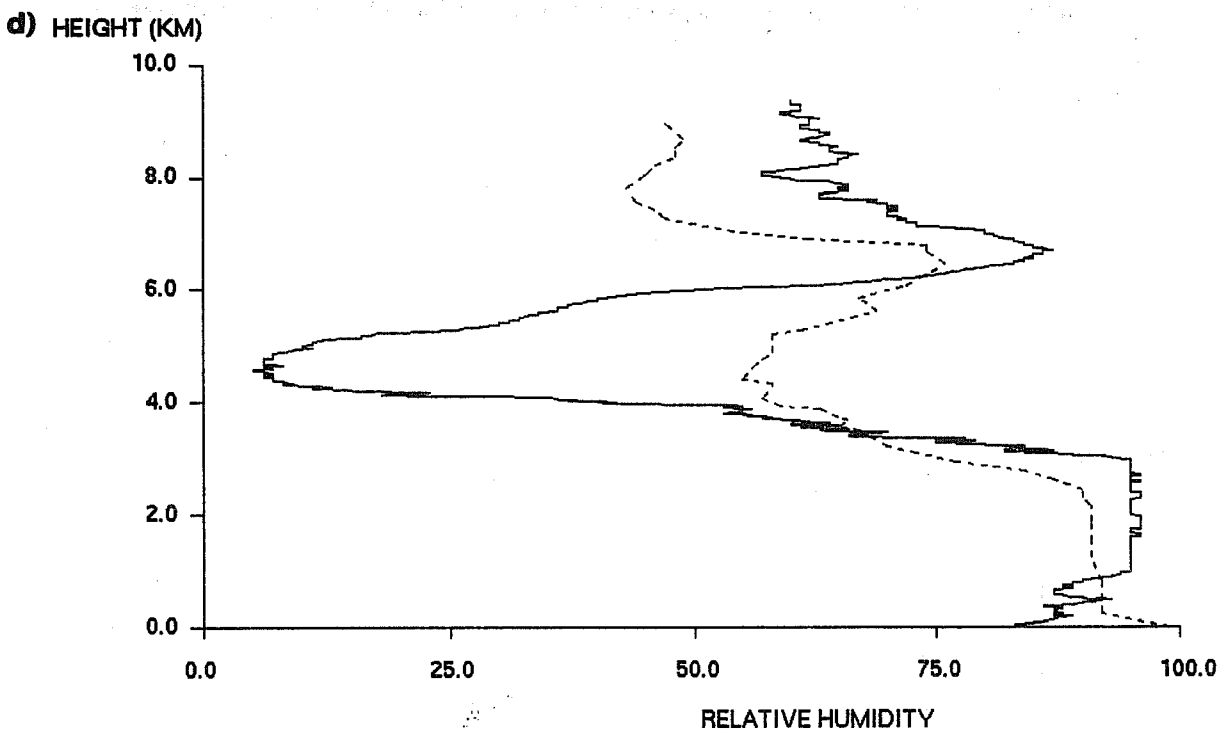

Fig. 2d)

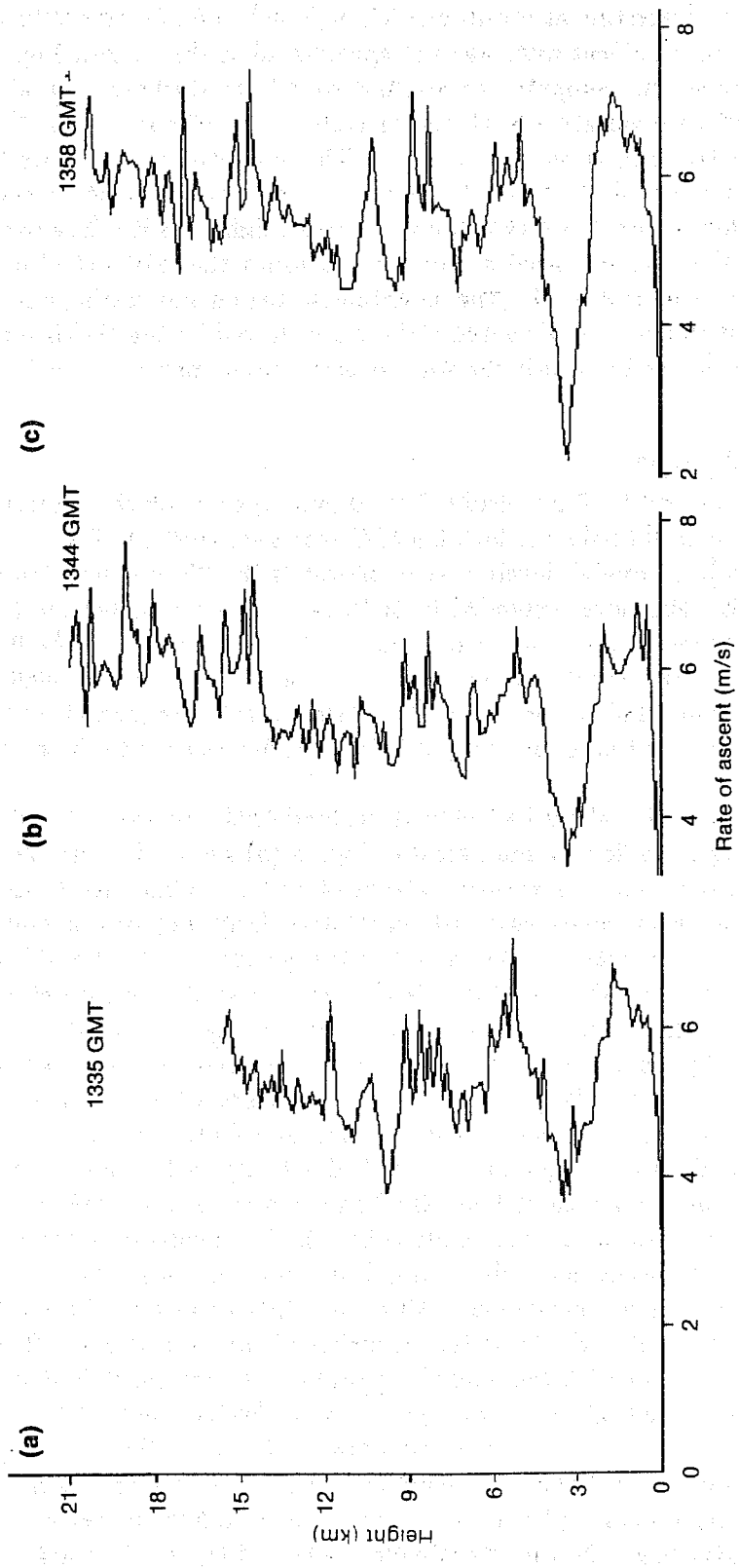

Fig. 3 Vertical profiles of ascent rate obtained from sondes released at (a) 1335 GMT, (b) 1344 GMT and (c) 1358 GMT.

stability of $\approx 1.6 \times 10^{-5}\ s^{-2}$ and considerably less stable above with tropopause at about 10 Km (Fig. 2 (a)). The wind speed is strong at most heights with a primary jet of 52 ms^{-1} at 10 Km and a secondary jet at about 2.5 Km (Fig. 2 (b)) : the wind direction veers gently with height throughout the troposphere.

Balloons were released at 1335, 1344 and 1358 GMT - each achieving a mean ascent rate of slightly larger than 5 ms^{-1} and bursting at pressures 12.4, 30.5 and 24.6 mb. respectively (N.B. the value of a wide range of mean ascent rates was not appreciated at this stage). Fig. 3 shows the ascent rates of the three sondes computed as averages over layer thicknesses of about 200 m. The peak-to-peak ascent rate variation in the lower troposphere of about 4 ms^{-1} implies a lee wave with vertical velocity amplitude of $\approx 2\ ms^{-1}$. The high level of coherence between ascent rate fluctuations over a period of 23 minutes is highly suggestive of a quasi-steady wave field. A downdraft approaching 3 ms^{-1} is attained just above a height of 3 Km The decrease in wave amplitude at heights above 10 Km need not necessarily imply the existence of a trapped lee wave since the sonde at this stage is leaving the mountainous region and passing out over the Midlands: a similar response might be anticipated if the waves forced by the Welsh mountains were untrapped hydrostatic waves for which the wave energy travels upward at only a small angle from the vertical.

2.2 Model configuration and results

The model was set up on a regular 3 Km grid (70 × 70 points) covering the greater part of Wales. The model orographic height field and location of Caersws are shown in Fig. 4 (contour int. 100 m; shaded > 400 m). 32 model levels were employed with 600 m separation above a height of 1.51 Km. The damping layer extended from 10.51 Km to the model top (at 17.11 Km) with horizontal diffusion increasing from a background value of 500 m^2s^{-1} to 25000 m^2s^{-1} at the model top. The Newtonian damping parameters τ_*, z_* and z_d were set to 9000s, 10.51 Km and 2 Km respectively. The wind on the lowest five levels was initially (and at all times on the lateral boundaries) set equal to that on level 6 (1.51 Km) which was close to the geostrophic value.

Following an adjustment period of about half an hour the model fields quickly settle down and after four hours the resulting wave field is quasi-steady. Fig. 5 (a) shows the vertical velocity at a height of 3 Km above sea-level . A regular pattern of bands extends across the whole mountainous area from north-west to south-east with particularly large amplitudes immediately downstream of Snowdonia. The vertical velocity amplitude is typically $\approx 2\ ms^{-1}$ and locally up to 6 ms^{-1} with a dominant wavelength of 22 Km. Vertical cross-sections were obtained along the line indicated in Fig. 5 (a); the vertical velocity is shown in Fig. 5 (b). Phase lines of the gravity wave are essentially vertical indicating some degree of trapping. The regularity of the wave field compared to the terrain height contour pattern suggests that this is a resonant response though further investigation shows only partial trapping (Shutts, 1992).

In order to verify the model wave response, the vertical velocity in the model was determined along the path of the sonde released at 1358 GMT and compared to the inferred vertical velocity derived from the rate-of-ascent of that sonde (Fig. 6). The model response compares favourably with the radiosonde ascent, not only in amplitude, but also in phase although the phase agreement deteriorates further downstream. Since the other two sondes have much the same ascent rate profiles there is little doubt of the reliability of the observations. The sonde observations therefore are consistent with the model's picture of a steady partially-trapped lee wave pattern with horizontal wavelength somewhat greater than 20 Km. Since the orography and the wave motion itself are both well resolved on the model's 3 Km grid, there is every reason to expect a realistic wave response. On the other hand the closeness of the agreement may be fortuitous since the treatment of damping layer/ upper lid is not ideal and the neglect of moist processes could be detrimental (e.g. Durran and Klemp, 1982). However, it was found that the inclusion of a realistic humidity profile made only a small reduction in wave amplitude and did not significantly detract from the good sonde *versus* model agreement found in the dry run.

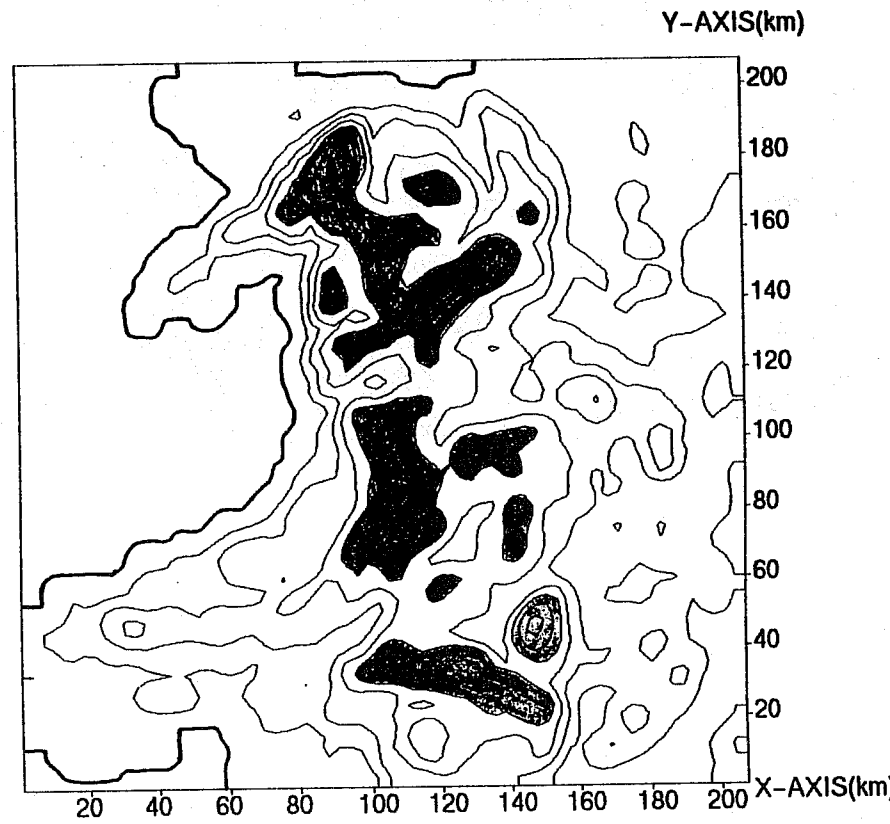

Fig. 4 Orographic height field used in the Mesoscale model. The cross marks the relative position of the field site at Caersws.

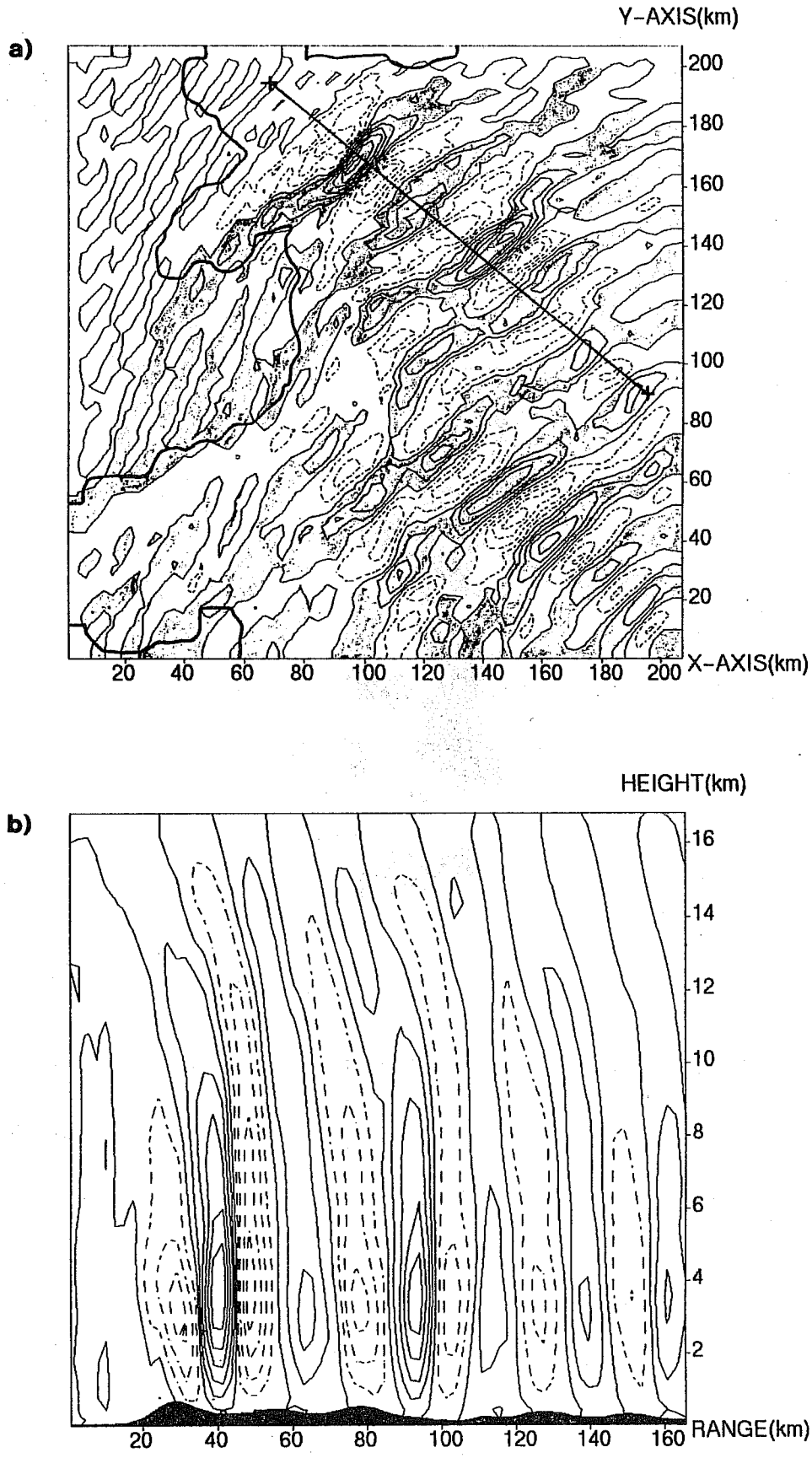

Fig. 5 (a) The Mesoscale model vertical velocity field at a height of 3 Km. above mean sea level after four hours of model integration. The line indicates the position of the vertical cross-section of vertical velocity shown in (b). The contour interval in both plots is 1.0 ms^{-1}.

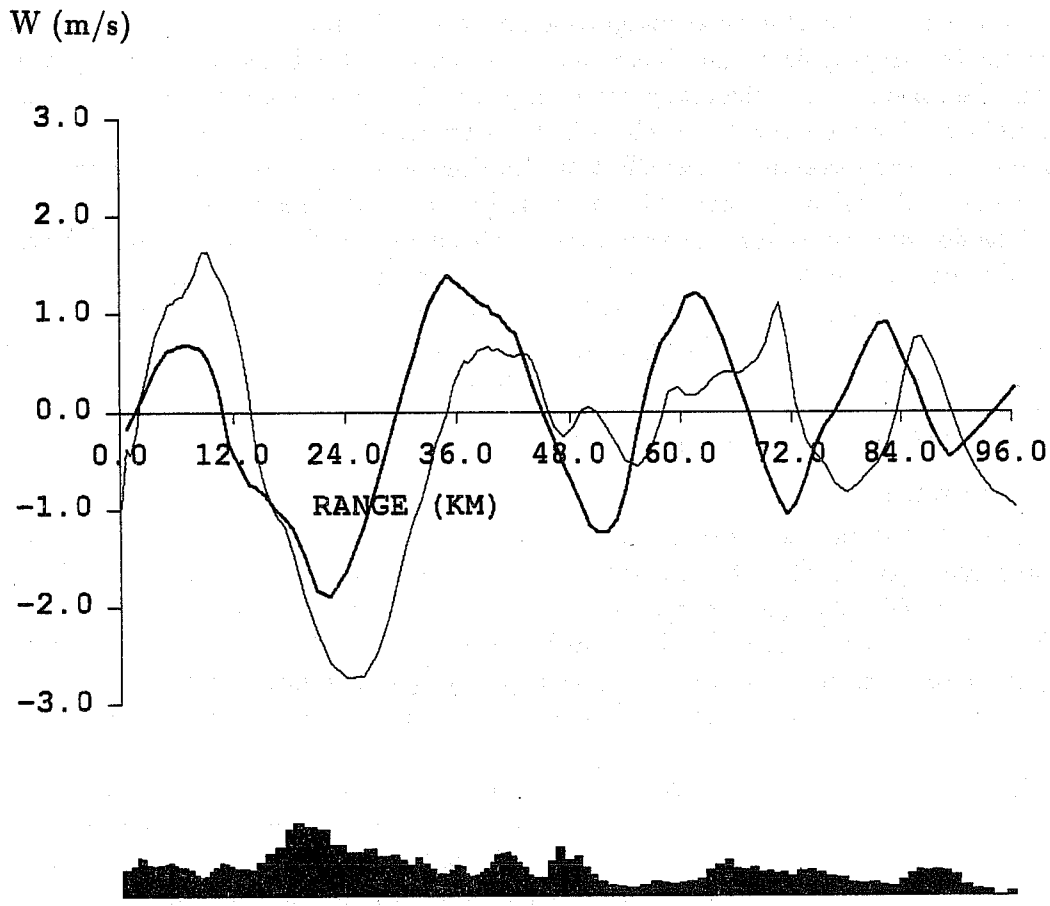

Fig. 6 Comparison of the vertical velocity inferred from the sonde released at 1358 GMT (thin line) with model vertical velocity (bold line) along the path of the sonde.

It is interesting to note that in four out of five case studies of trapped lee waves in the U.K., Brown (1983) found that dry, linear theory appeared to satisfactorily predict their wavelength and vertical structure.

It should be noted that the model simulation shown here is not the same as that appearing in Shutts (1992) which had 19 model levels and a different representation of the vertical momentum equation. Also the surface geostrophic wind speed is stronger in this experiment and $\approx$ 23.5 ms^{-1}.

Computation of the orographic pressure force F on the orography is given by:

$$F = \int\int_{\mathbf{D}} \left(p\frac{\partial E}{\partial x}, p\frac{\partial E}{\partial y} \right) dx\, dy \tag{3}$$

(where subscript **D** denotes integration over the entire model domain) is complicated by the fact the the orographic height $E(x, y)$ does not vanish at the boundaries leaving a contribution even when there is no horizontal pressure gradient. The basic state horizontal pressure gradient exerts a *lift* force on the orography which contributes to the above expression. In order to compute a drag force due to the effect of forced lee waves alone we have chosen to subtract off the value of F evaluated when only the basic (initial) state pressure field is present.

The domain averaged surface pressure drag contribution from the forced lee waves was computed to be (0.46, -0.21) Nm^{-2} - a sizeable force. Net surface frictional stress was also computed as a domain averaged vector and was found to be (1.16, -0.67) Nm^{-2}, considerably more than the pressure drag force but in agreement with recent measurements made in the Welsh field experiment reported by Grant and Mason (1990).

3. SCOTTISH CASE STUDY - OCT. 12 1990

3.1 Observations

The Scottish field experiment was conducted by the Meteorological Office's Cardington research group and held at the eastern end of Loch Cluanie in West Scotland. The mountains here are considerably more rugged than in Wales with peak heights near the field site of 1.2 Km. In this instance, the sonde data was being collected to study boundary layer structure over the mountains rather than gravity waves and multiple soundings were not required. Even so, several excellent lee wave events were identified in single soundings with wave amplitudes of 2 to 3 ms^{-1}.

The lee wave event under consideration here occurred on Oct. 12 1990. A mild south-southwesterly airstream covered Scotland at midday with a quasi-stationary front over the Western Isles. The NOAA 11 polar orbiter satellite at 1313 GMT shows a complex pattern of lee waves with a variety of wavelengths and orientations. Near the field site, lee wave cloud bands are oriented E by N to W by S and with a wavelength of 9 to 12 Km. Fig. 7 shows the wind and temperature profile at 1053 GMT together with the ascent rate *versus* height. The wind speed increases steadily with height from a surface value of $\approx$ 7 ms^{-1} to 43 ms^{-1} at about 7 Km. The wind direction is essentially constant with height above 2 Km at 212°. The temperature inversions near 2 and 5 Km may well be spurious and due to horizontal temperature variation in the lee wave sampled as the sonde ascends slowly in downdraughts.

A regular pattern of waves with vertical velocity amplitude $\approx$ 2 ms^{-1} above a height of 2 Km is suggested by the ascent rate variations. If the phase lines are assumed to be vertical, the horizontal distance between successive ascent rate troughs gives some measure of the horizontal wavelength along the sonde trajectory. The ascent rate minima between 2 and 7 Km are found to be spaced at intervals of 16, 17.5 and 19.5 Km successively as one goes upward. Of course these distances are not true wavelengths since the sonde travels at about 40° to wavevector orientation as determined from satellite pictures. The true wavelength then lies in the range 12

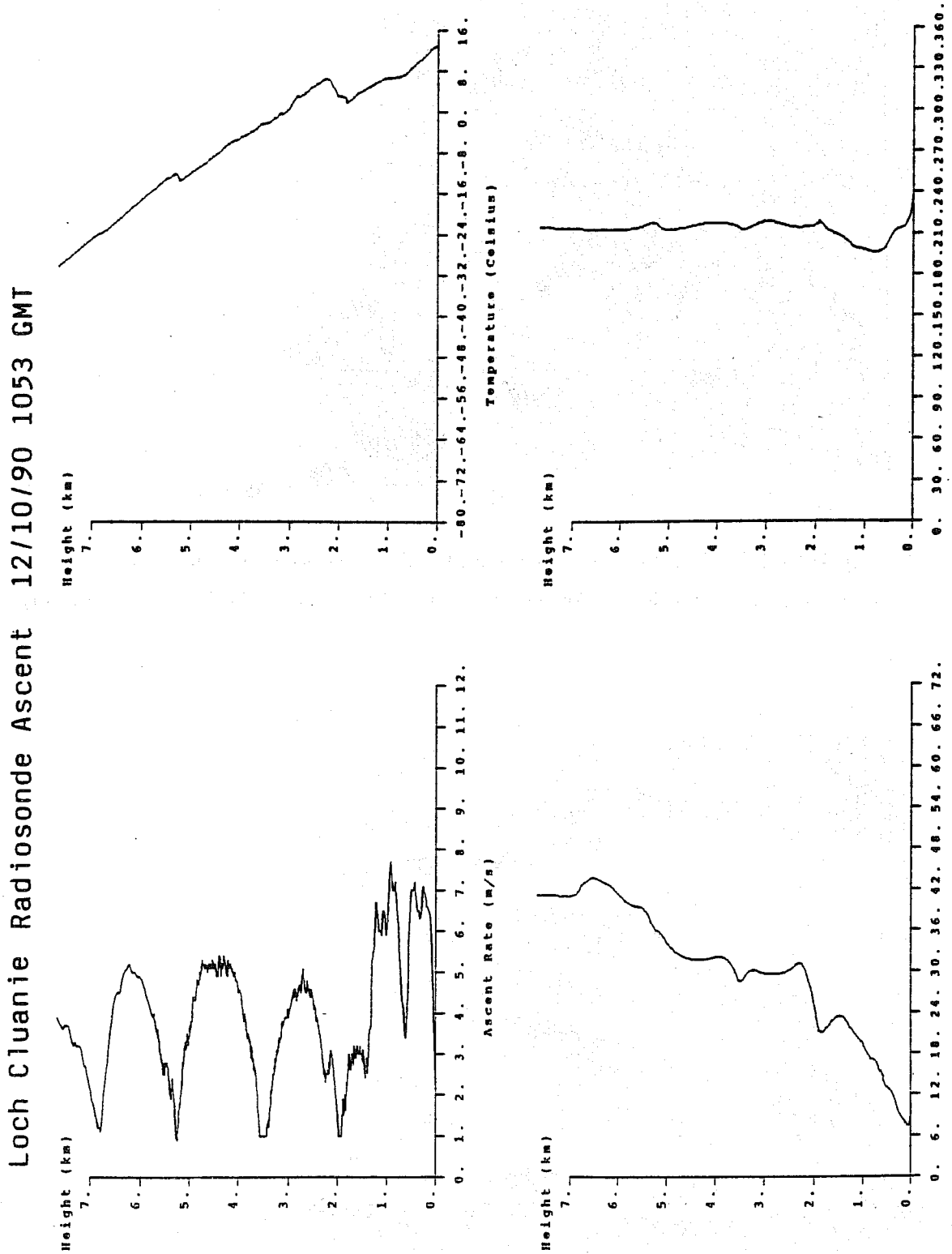

Fig. 7 Vertical profiles of wind speed and direction, temperature and ascent rate obtained from the sonde released at 1053 GMT from Loch Cluanie.

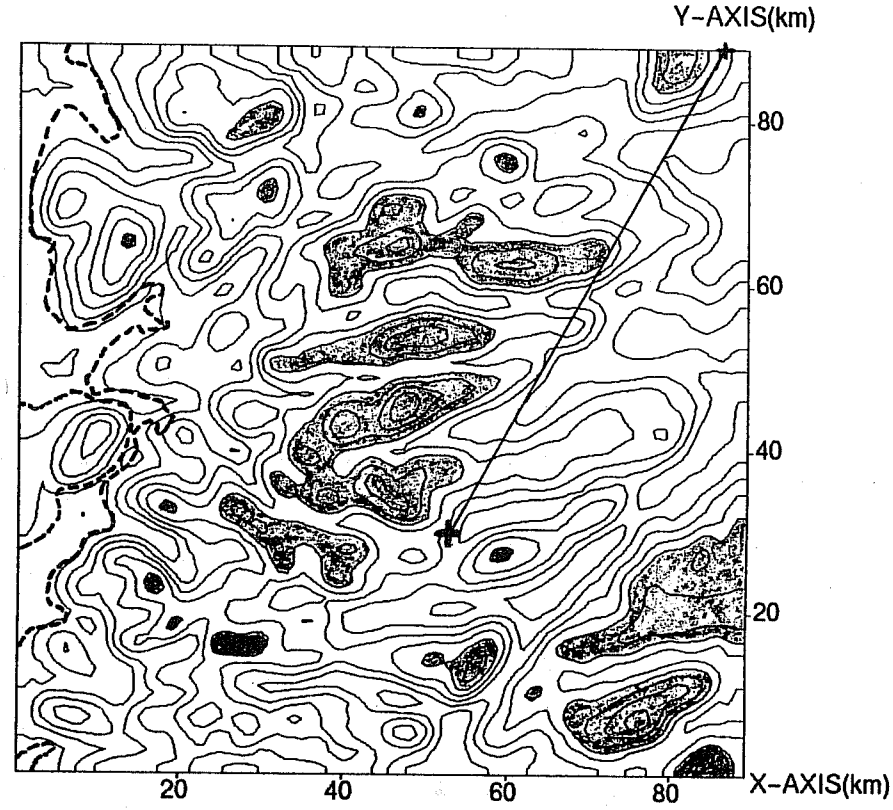

Fig. 8 Orographic height field used in the Mesoscale model. The cross marks the relative position of the field site at Loch Cluanie. The line indicates the position of the vertical cross-section in Fig. 10.

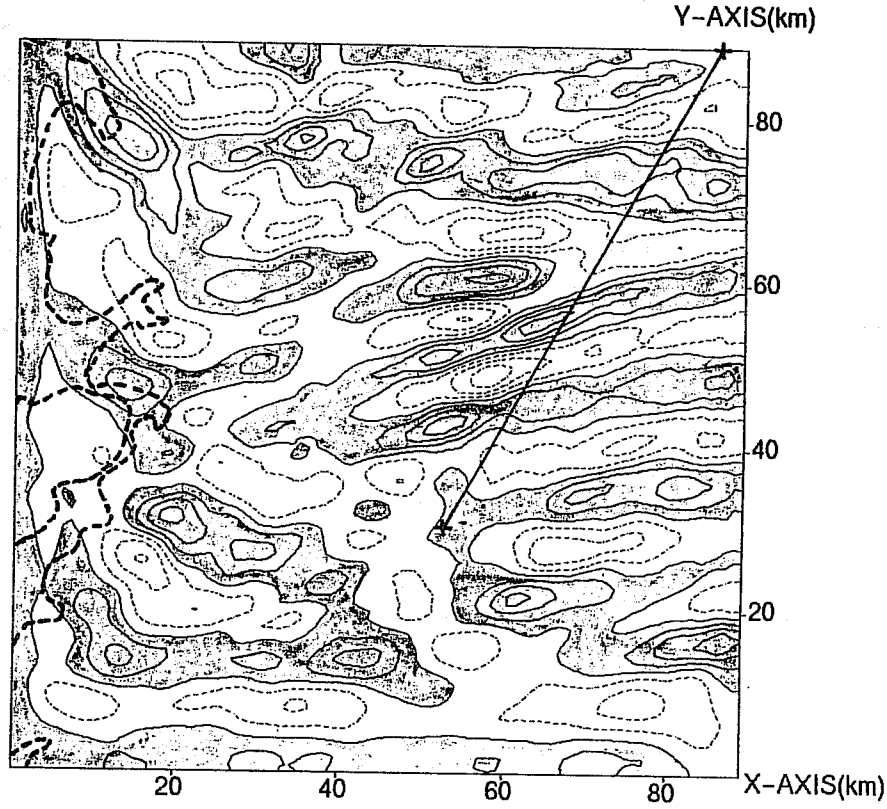

Fig. 9 Model vertical velocity field at $z = 3\ Km$ after four hours of integration. The line indicates the position of the vertical cross-section in Fig. 10. Contour interval: 1 ms^{-1}.

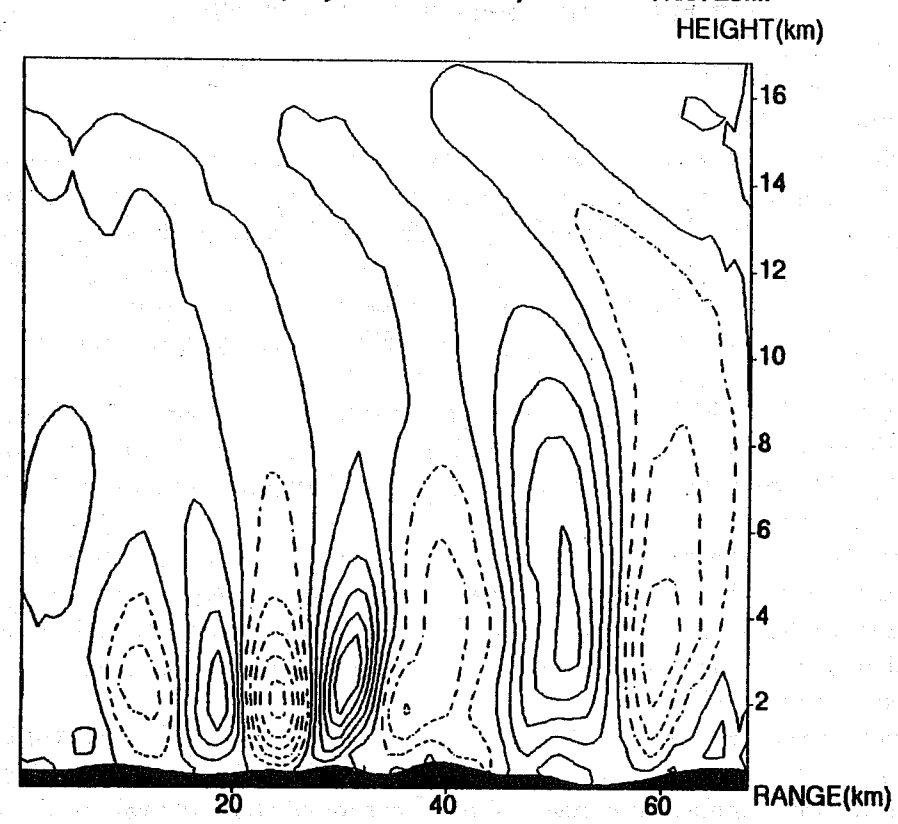

Fig. 10 Vertical cross-section of vertical velocity along the line indicated in Fig. 9. Contour interval: 0.5 ms^{-1}.

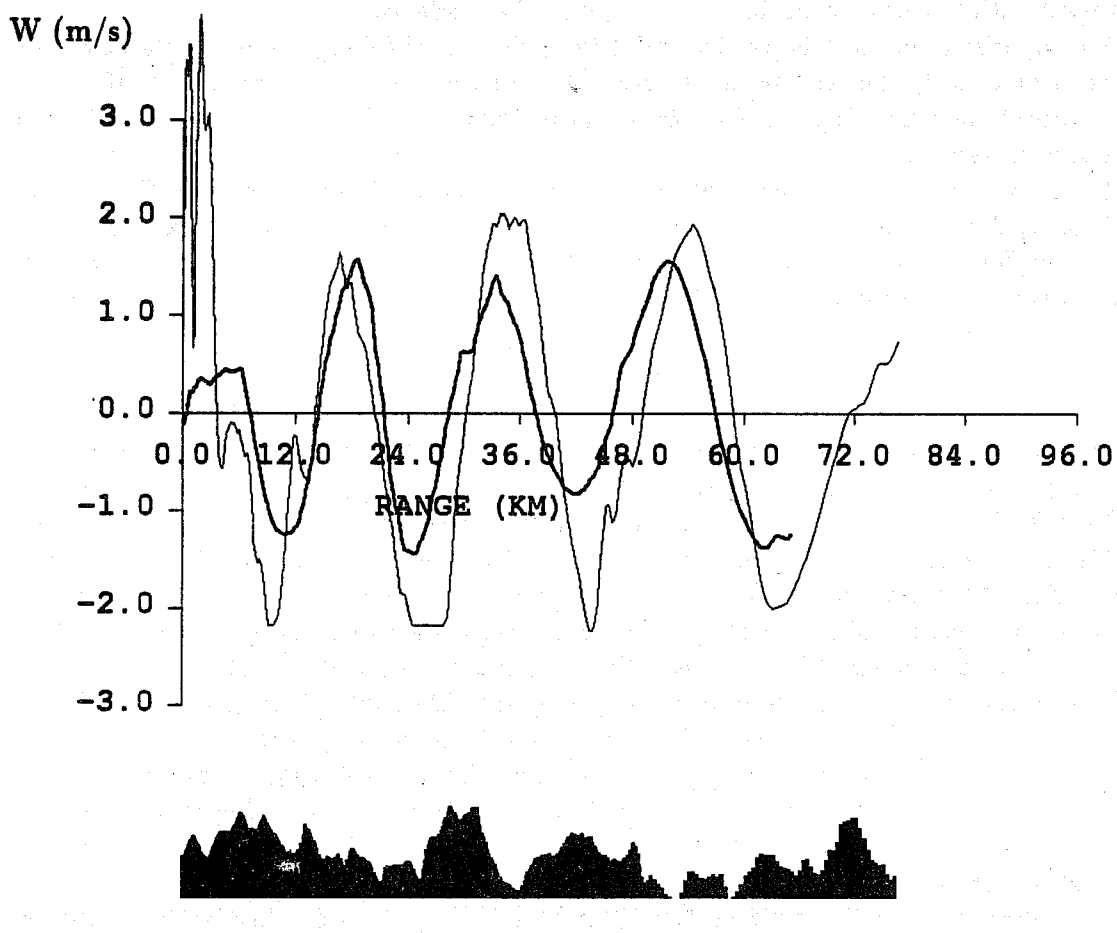

Fig. 11 Comparison of the vertical velocity inferred from the sonde released at 1053 GMT (thin line) with model vertical velocity along the path of the sonde (thick line).

and 15 Km - somewhat longer than that implied by the 1313 GMT satellite picture.

3.2 Model configuration and results

Although the model level distribution was the same as that used in the Welsh case study, a 1 Km grid was chosen in view of the 10 Km wavelength apparent in the satellite imagery and the shorter orographic ridge/valley spacing near Loch Cluanie. It was also found necessary to use somewhat higher horizontal diffusion below the stratospheric damping layer due to the steeper mountain slopes. This was implemented in the numerical scheme by increasing the ratio of $\frac{\nu}{\Delta^2}$, where Δ is the horizontal gridlength. The horizontal diffusion coefficients ν were set at a base value of 500 m^2s^{-1} below z_* (= 10.51 Km), rising to 5000 m^2s^{-1} at the top of the model. The model orography covering a 90 Km square region is shown in Fig. 8 (contour int. 100 m; shaded > 600 m) together with a line along which vertical cross-sections are taken (approximately along the sonde path). The roughness length z_0 over land was here set proportional to the terrain height such that a maximum value of 3 m occurred over the highest peak.

A compromise has to be achieved between the smallness of the gridlength required to resolve the lee wave and the areal extent of the domain required to encompass the sonde path and sufficient upstream fetch. Since highly-trapped lee waves may extend hundreds of kilometres downstream of orographic features, the local wave response may be influenced by upstream orography outside of the model domain.

The quasi-steady vertical velocity field at a height of 3 Km and four hours into the simulation is shown in Fig. 9. The wave field is complex and clearly dependent on the local underlying terrain. Maximum wave amplitudes of nearly 4 ms^{-1} are found and a typical wavelength would be 10 Km. A vertical cross-section of vertical velocity taken along the line indicated in Fig. 9, and whose point furthest upstream corresponds to Loch Cluanie, is shown in Fig. 10. It shows a pattern of waves which increase in horizontal wavelength and vertical extent downstream - consistent with the wavelength increases noted in the sonde ascent rate.

A comparison between the vertical velocity in the model (along the sonde trajectory) with the vertical velocity deduced from the variation of ascent rate (by subtracting off the mean ascent rate) is shown in Fig. 11. The agreement is again very good, particularly in the apparent horizontal wavelength.

The resultant wave drag vector after four hours of integration was found in this case to be (0.19, 0.44) Nm^{-2} - a considerable force compared to a typical boundary layer surface shear stress over *flat* terrain but small compared to the domain-averaged surface frictional drag force found in this model simulation, i.e. (1.09, 2.42) Nm^{-2}.

4. LAKE DISTRICT CASE STUDY - NOV.26 1991

4.1 Observations

The lee wave event which forms this case study occurred on the afternoon of November 26 1991 over the Lake District and Northern Pennines of England . The sea-level pressure analysis at 14 GMT (Fig. 12) shows a southwesterly airstream ahead of a minor polar airstream trough. At this time the trough is less than 100 Km from the sonde release station Eskmeals (located at E in Fig. 12; Cumbria is shaded) and is rather weak. The surface geostrophic wind speed ahead of the trough is about 17 ms^{-1} which implies substantial orographic forcing of vertical motion. Vertical profiles of wind speed, direction and temperature are shown in Fig. 13 (a) - (c) respectively. They are derived from a composite of an upstream aircraft profile and a radiosonde released from Eskmeals. The wind speed increases to $\approx 41ms^{-1}$ at about 9 Km - close to the height of the tropopause. The wind direction is southwesterly throughout most of the troposphere but like the wind speed, oscillates in the stratosphere due to the presence of gravity waves. The temperature variation below 1.3 Km is close to the dry adiabatic value and rather stable above that up to a height of 4 Km.

A satellite photograph (not shown) at 1422 GMT shows extensive low-level cloud over the Irish Sea and near the Cumbrian coast. Cloud bands with a range of orientations about NW -

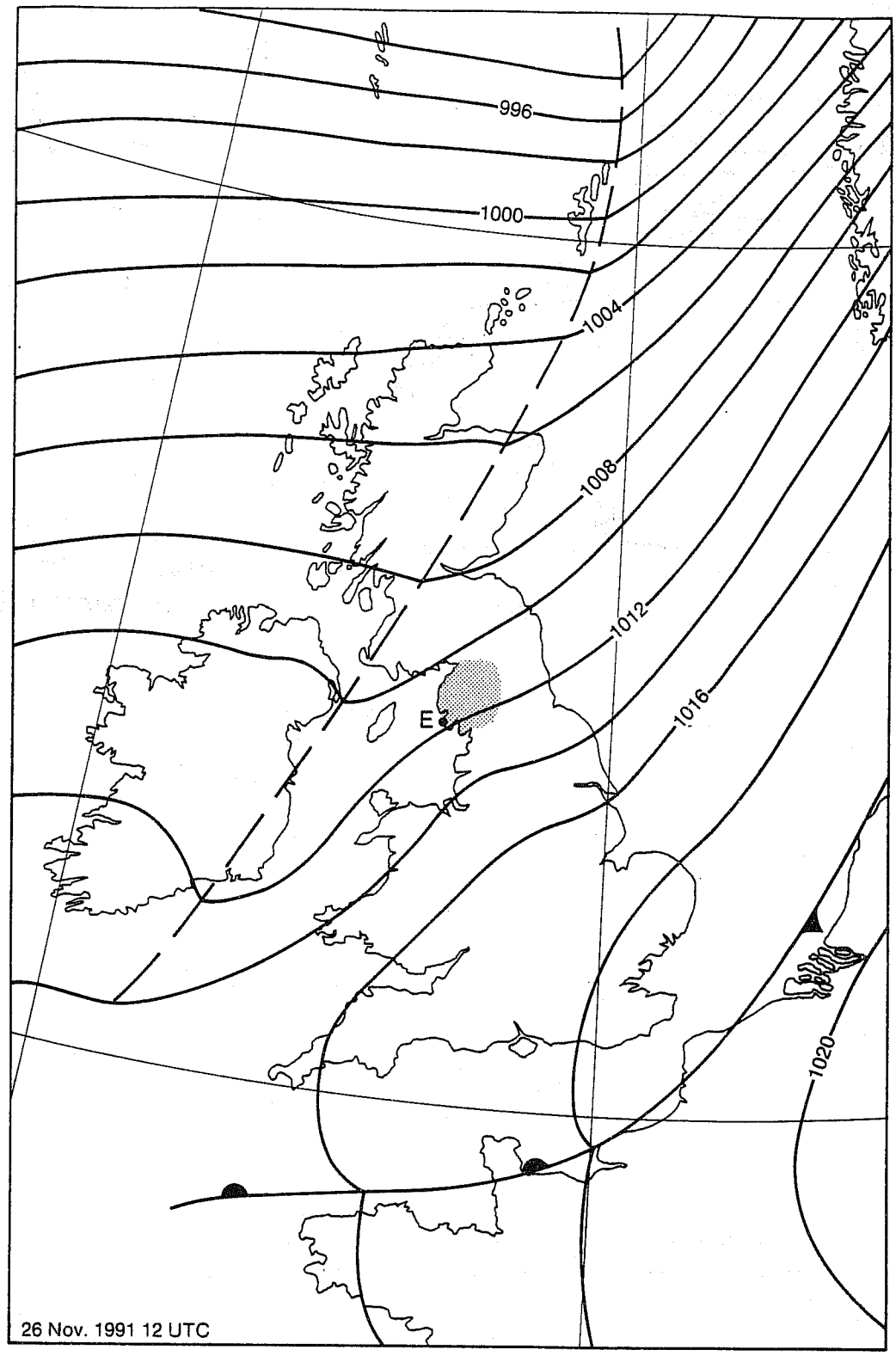

Fig. 12 Sea-level pressure analysis at 14 GMT. The Lake District is shaded and the location of Eskmeals is identified with an E.

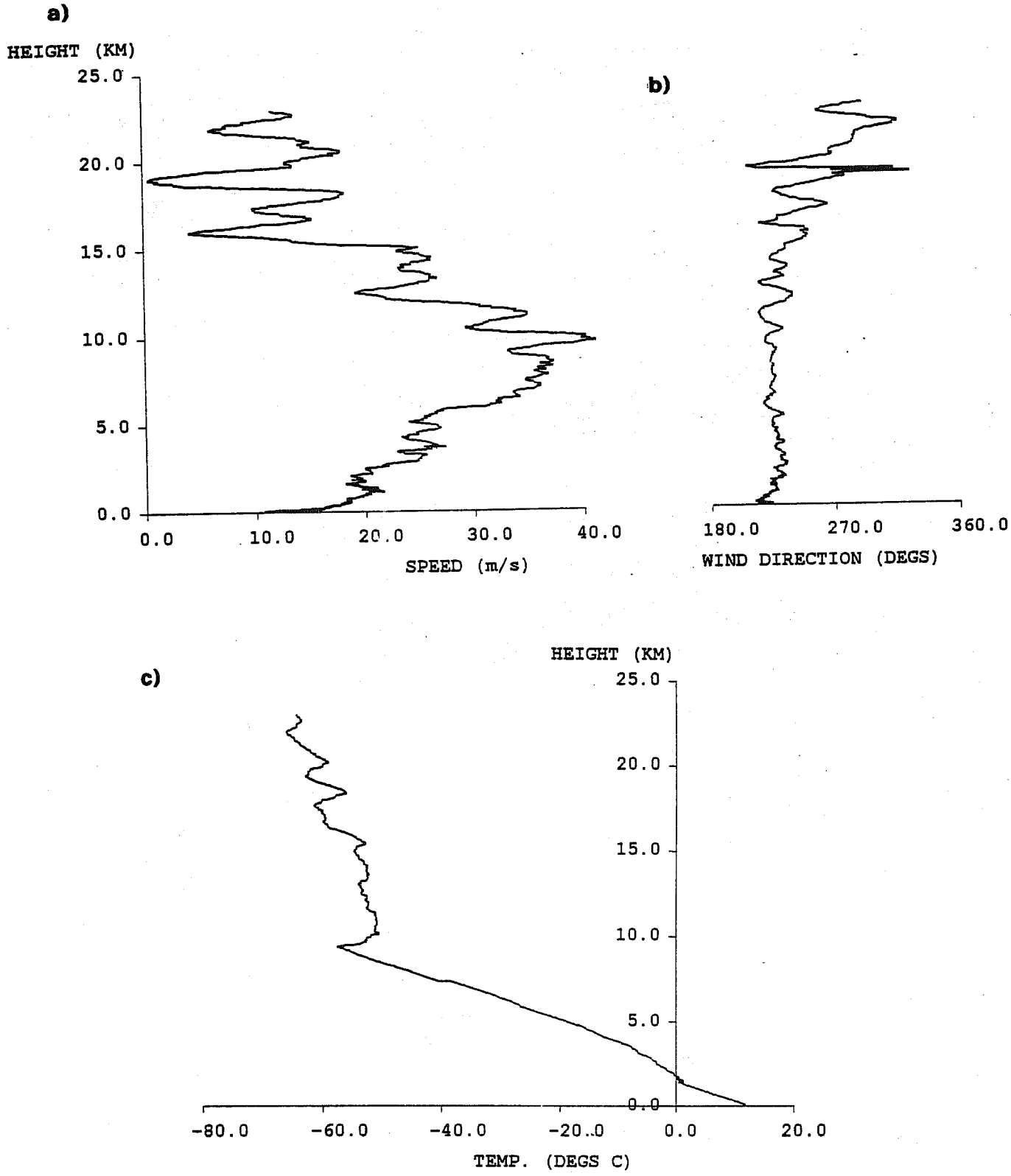

Fig. 13 Vertical profiles of (a) wind speed, (b) wind direction and (c) temperature obtained from the aircraft descent profile below 7.3 Km and sonde E above.

SE can be seen over the Lake District and further downstream : these we take to be the visible manifestation of lee waves. The spacing between the bands is also rather variable but generally around 20 Km.

On the afternoon of November 26 1991, five sondes labelled **A** to **E** were released from Eskmeals at times 1359, 1407, 1412, 1419 and 1426 GMT respectively. Fig. 14 shows the vertical velocity measured by each of the five sondes plotted against distance downstream. The lee wave is most noticeable in sondes **A** and **B** which stayed at low levels for longer because of their smaller mean ascent rates. A peak vertical velocity amplitude of at least 3 ms^{-1} is evident with pronounced downdraughts at ranges of 20 and 40 Km. Further aspects of the radiosonde data will be discussed later.

The aircraft experiment consisted of four level flight legs of length $\approx$ 160 Km oriented essentially NE to SW and at heights of 2.35, 3.69, 5.52 and 7.35 Km (Runs 1 to 4 respectively). Run 1 began at 1320 GMT and Run 4 finished at 1525 GMT. Prior to these level runs, a descent profile was obtained over the Irish Sea from 7.35 Km down to 16 m above sea level to serve as an 'undisturbed' upstream profile. This was obtained between 1243 GMT and 1308 GMT - about one hour before the first sonde was released. Fig. 15 shows the location of the descent profile run which begins just north of Anglesey, flying northeast to arrive near Eskmeals at a height of 3 Km and then looping back in descent towards sea-level. Also shown is the trajectory of sonde **A**. The horizontal paths of Runs 1 to 4 are omitted since they, together with all five sondes, lie within a corridor $\approx$ 10 Km wide and, on average, much closer than this ($<$ 5 Km apart). The closeness of sonde and aircraft paths provides some assurance that a composite of the data can be used to analyse (in vertical cross-section) the wave motion.

Fig. 16 shows the vertical velocity inferred from the four level flight legs with the mean removed. The first thing to notice is that the greatest wave amplitudes are to be found on the lowest two flight legs and with 3 ms^{-1} amplitude are similar to the sonde ascent rate fluctuations about the mean. Vertical coherence in the vertical velocity is readily detectable on the lowest two flight levels but is harder to see higher up. At low levels around 70 to 100 Km downstream of Eskmeals, the vertical coherence also seems to be lost. We assume that this is primarily due to transience since the aircraft takes about half an hour to get from this region on Run 1 to the same area on Run 2.

Vertical velocity deduced from the five sondes and all four aircraft legs has been plotted on a vertical cross-section along a line extending northeastwards from Eskmeals (positions are projected normally onto this line). Sonde information is found to successfully complement the aircraft-derived vertical velocities and the resulting hand-analysis is presented in Fig. 17. This clearly shows the existence of a trapped lee wave pattern with considerable amplitude modulation in sympathy with the underlying orography. The dominant horizontal wavelength is approximately 20 Km and the amplitude of the wave has a maximum at a height of about 3 Km with vertical velocities of up to 3.5 ms^{-1}. Above 5 Km the wave amplitude becomes small and the phase lines have an upstream tilt with height consistent with upward energy leakage to the stratosphere.

4.2 Model results

For this case study the model was set up on a 2 Km grid with 43 levels extending up to a height of 23.11 Km (600 m separation above 1.51 Km as for both the previous case studies). The model orography is shown in Fig. 18 (contour int. 500 m; shading $>$ 500 m). The top 4.8 Kilometres were used as a damping layer with horizontal diffusion values increasing from a base value of 500 m^2s^{-1} to 25000 m^2s^{-1} at the model top, and Newtonian damping parameters τ_*, z_* and z_d set to 9000s, 18.31 Km and 1.6 Km respectively. The roughness length was prescribed in the same way as the previous case with peak values of 3 m.

A four hour model integration was carried out by which time the resulting wave field was virtually steady (i.e. differences between plotted vertical velocity fields for four and six hour integrations were negligible). The vertical velocity at a height of 3 Km (Fig. 19) shows a

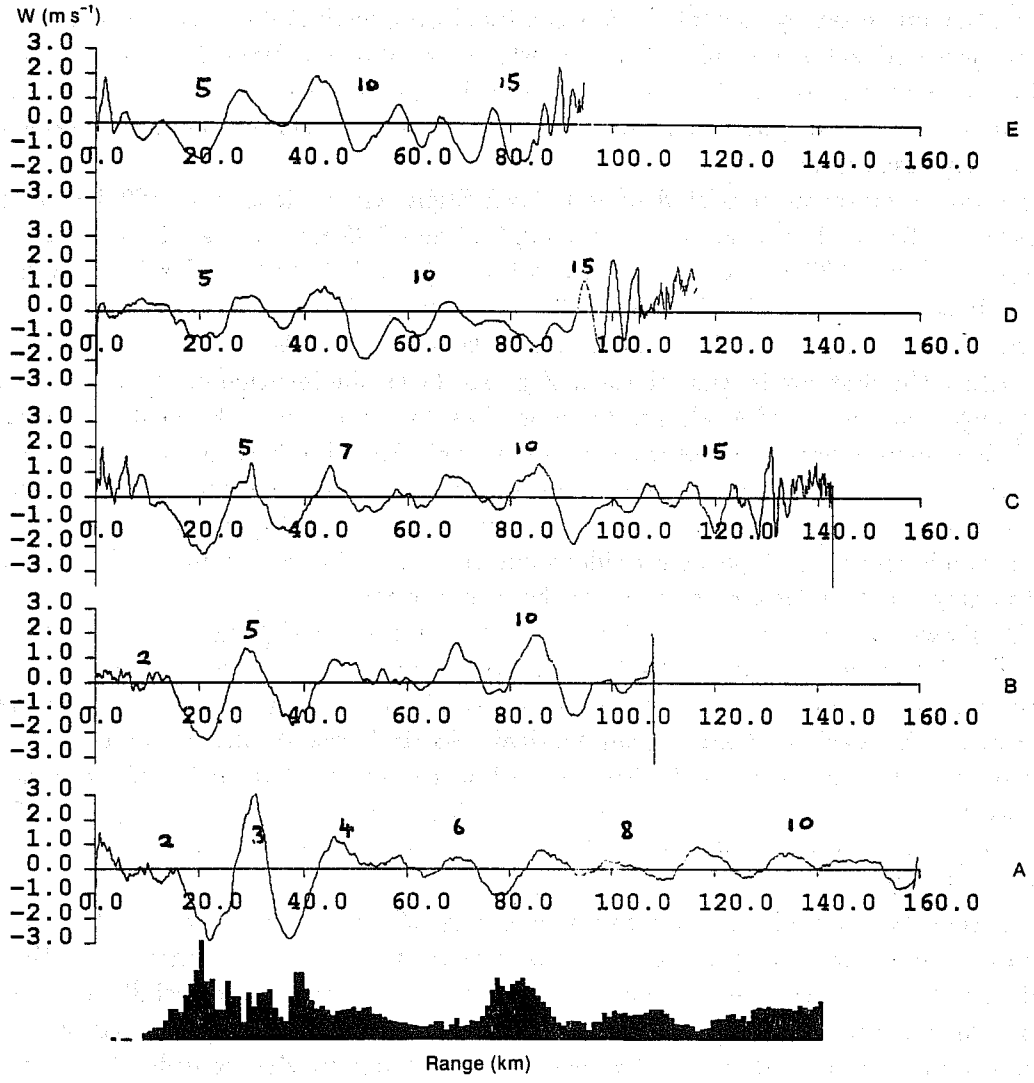

Fig. 14 Vertical velocity deduced for each sonde plotted above the orography in order of increasing mean ascent rate. The numbers entered beside each curve give the height of the sonde in Km.

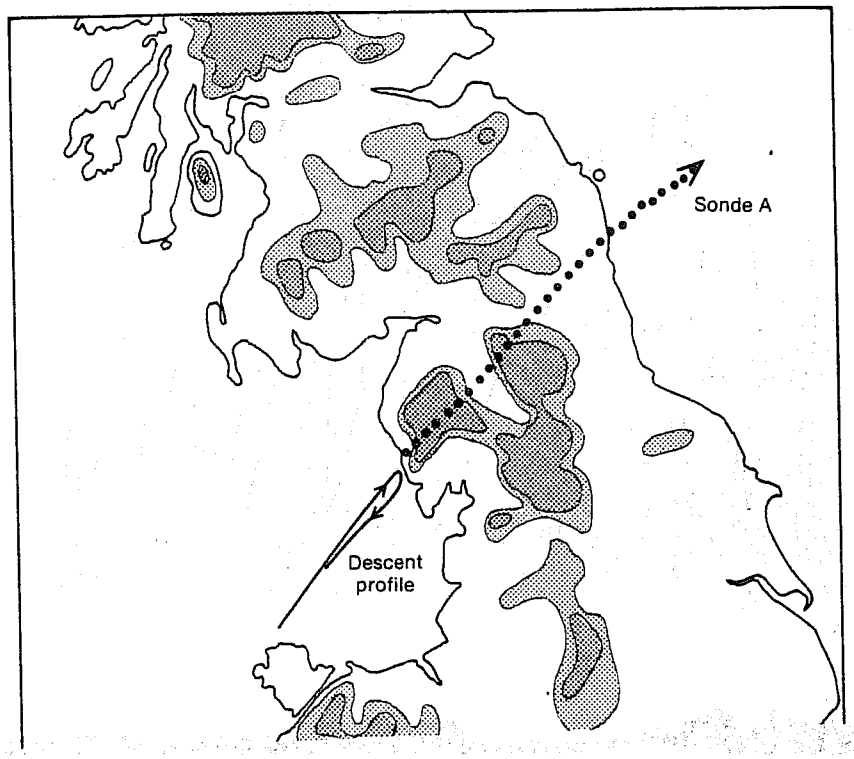

Fig. 15 Map showing the horizontal paths of the aircraft on the descent flight leg over the sea (*solid* line) and sonde **A** (*dashed* line).

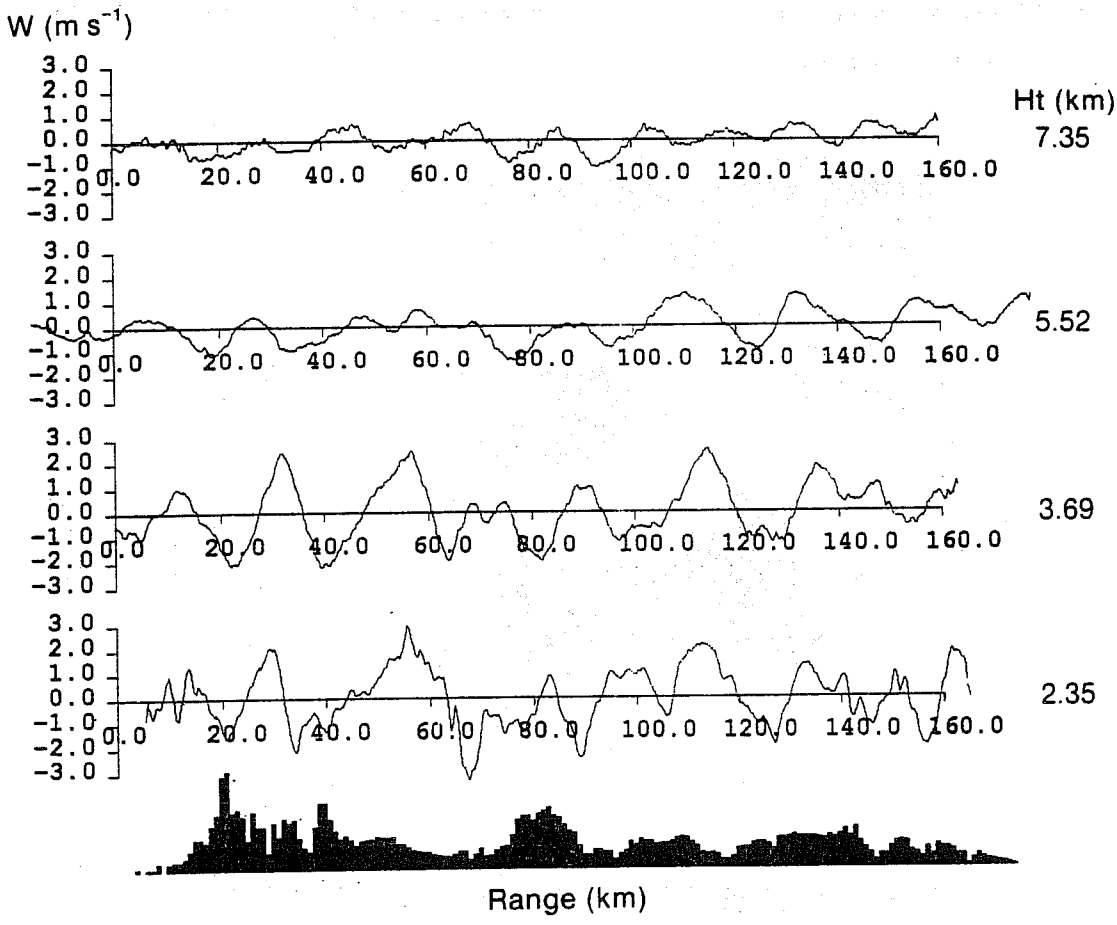

Fig. 16 Vertical velocity measured along the four aircraft flight legs. The mean on each leg was removed.

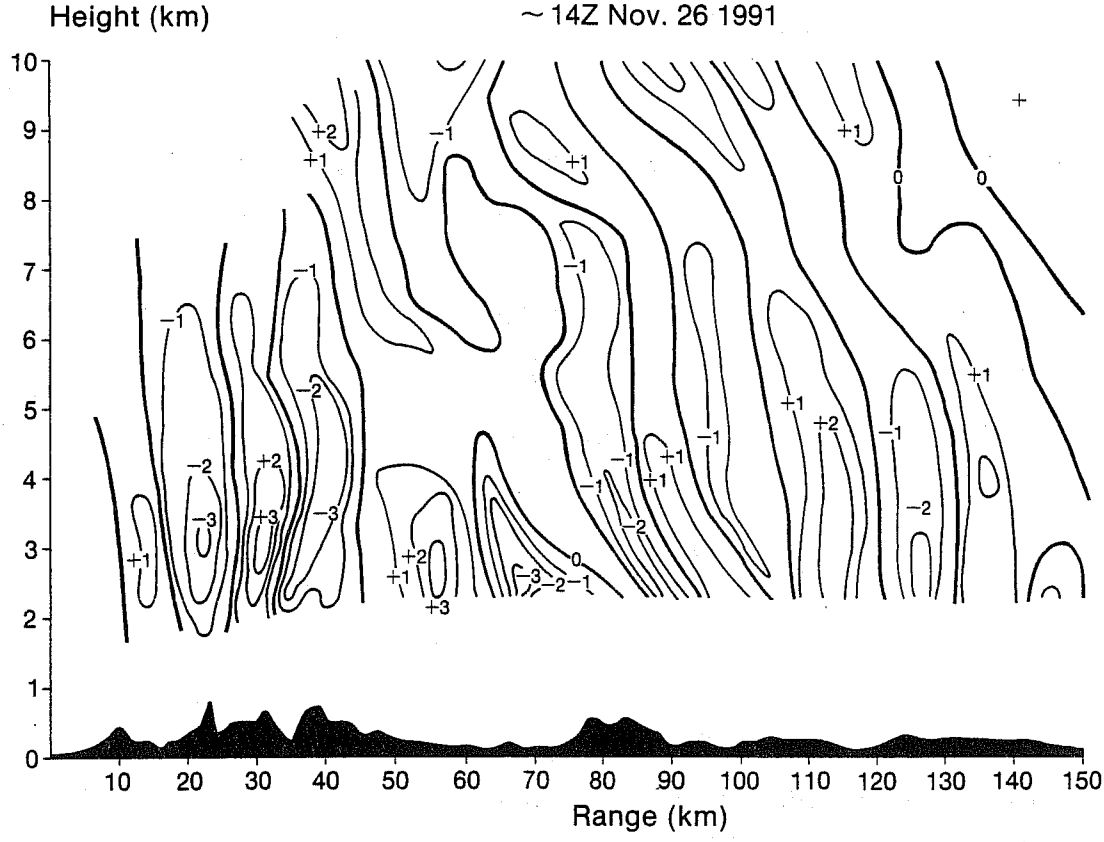

Fig. 17 A subjective analysis of the vertical velocity in the vertical plane oriented at 42° and passing through Eskmeals.

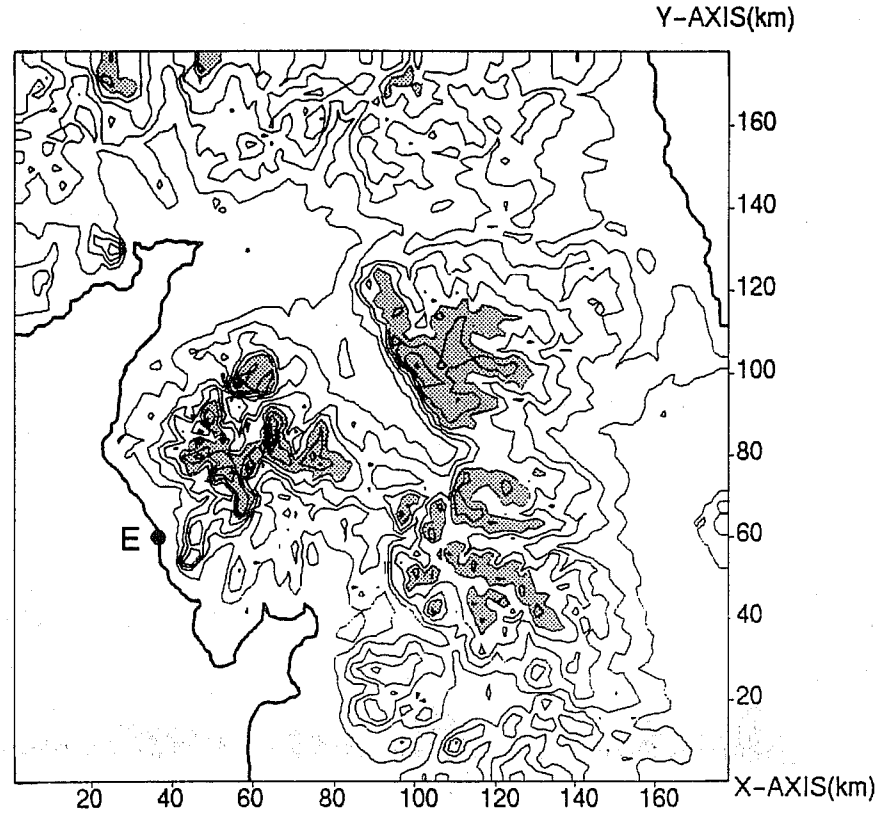

Fig. 18 Model terrain height map showing the real coastline in bold line and height above 500m is shaded. E marks the field site location, Eskmeals.

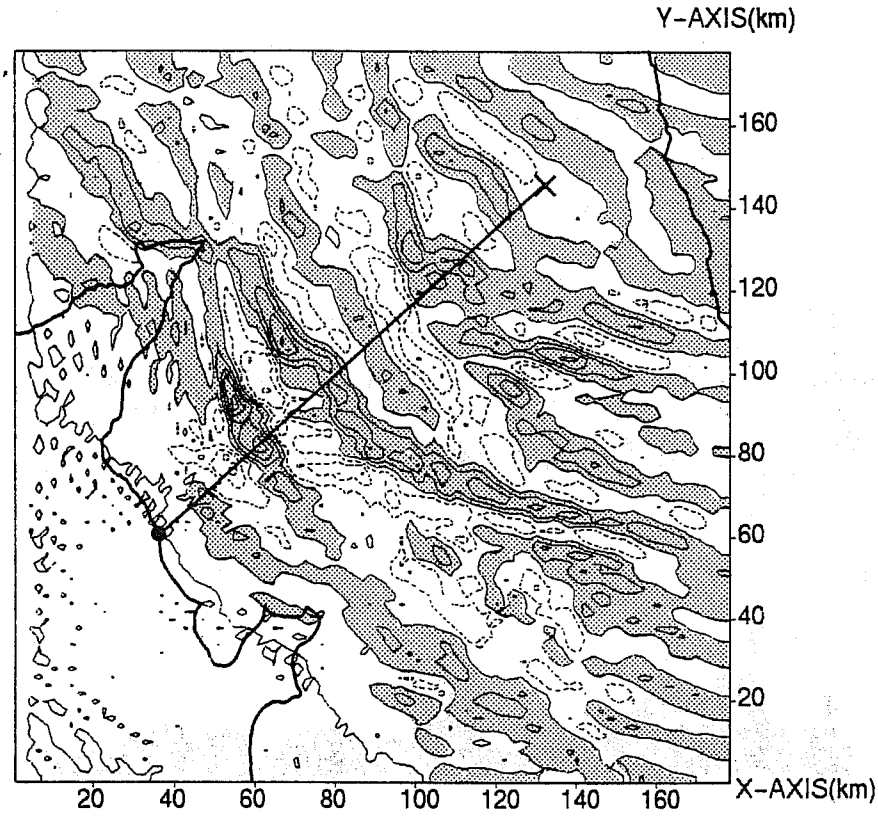

Fig. 19 Model vertical velocity field at $z = 3\ Km$ after four hours of integration. The line indicates the position of the vertical cross-section in Fig. 20. Contour interval: 1 ms^{-1}.

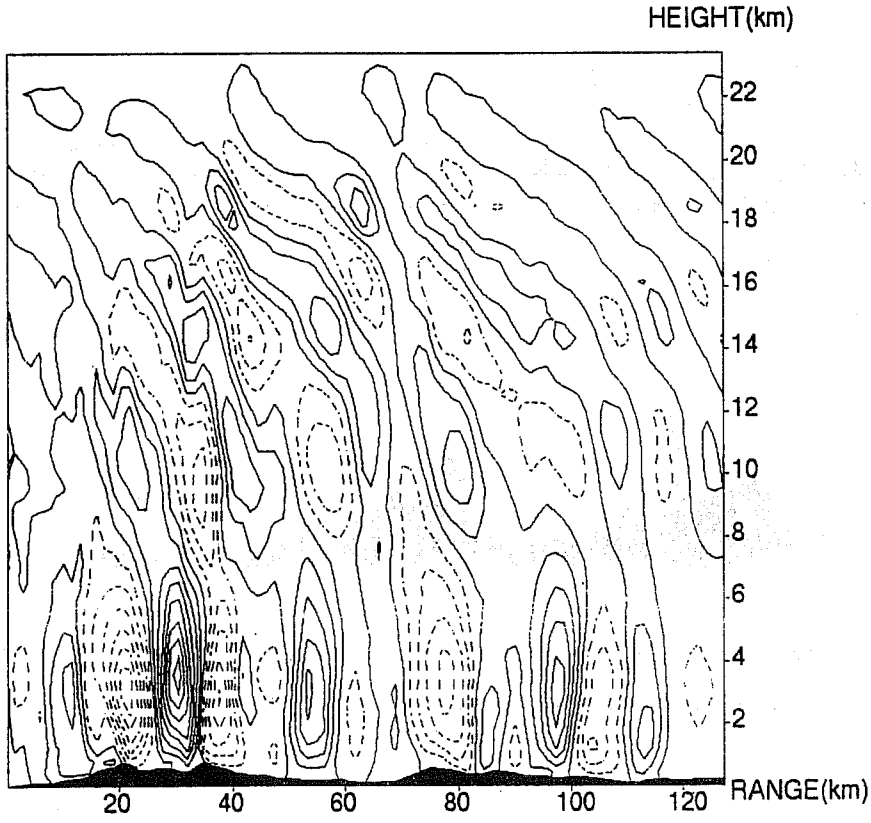

Fig. 20 Vertical cross-section of vertical velocity along the line indicated in Fig. 19. Contour interval: 0.5 ms^{-1}.

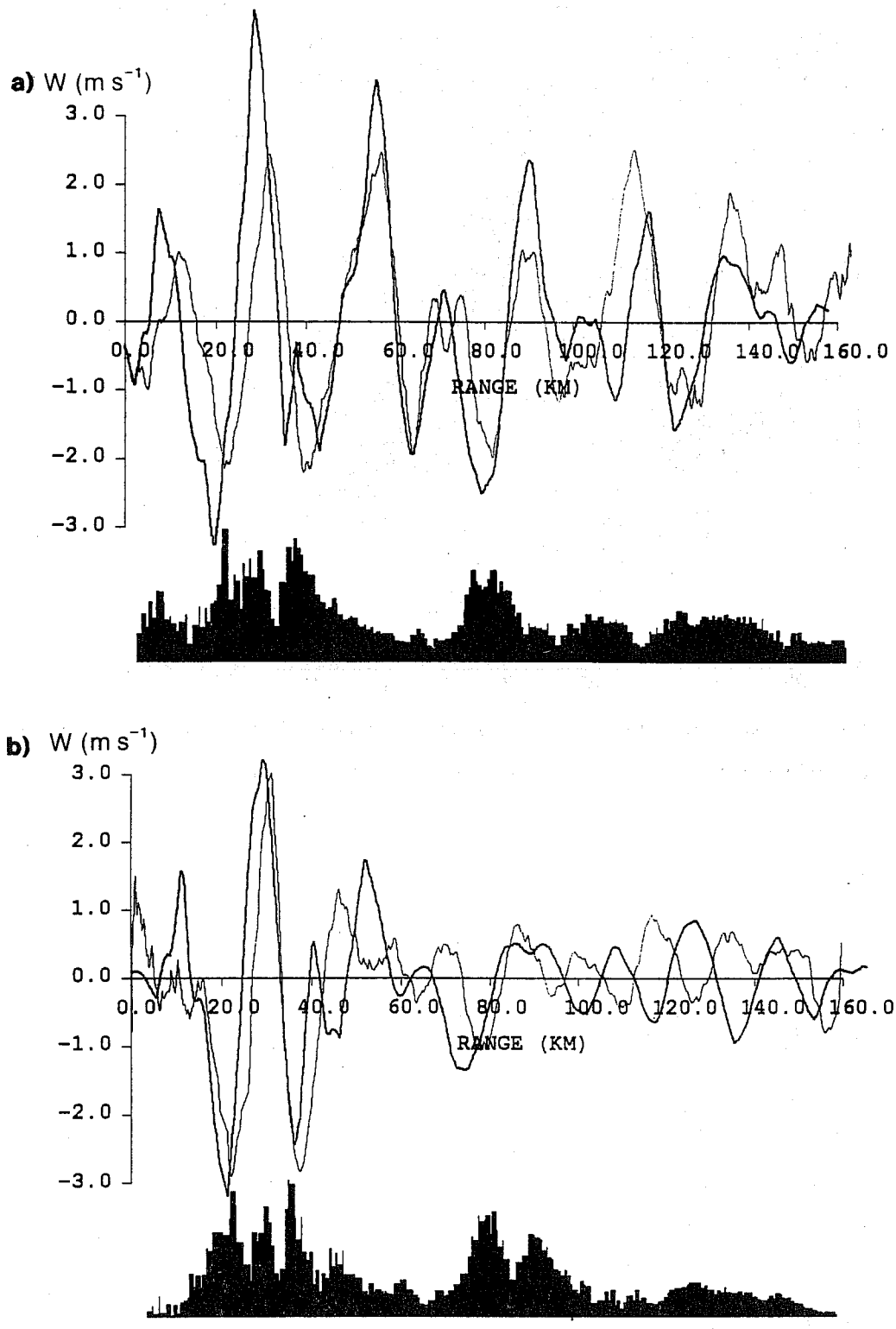

Fig. 21 Vertical velocity along the second aircraft flight leg (a) and sonde A (b) (thin lines) compared to that found along the equivalent paths in the model (bold lines).

fairly complex banded pattern over much of the land in the model domain and with a dominant wavelength of around 20 Km. Vertical velocities range between -3.6 and +4.7 ms^{-1} and are largest over the Lake District mountains.

A vertical cross-section taken along the line indicated in Fig. 19 is shown in Fig. 20. Comparing this with the hand-analysis of vertical velocity (Fig. 17) reveals a high level of agreement and the positions of individual updraughts or downdraughts with respect to the orography can be seen to correspond (e.g. the first two descent regions downwind of Eskmeals occur just to the lee side of the Scafell and Helvellyn mountains respectively) . The dominant wavelength, as seen in the w map at a height of 3 Km, is about 20 Km and the extreme values +3.7 and -3.2 ms^{-1} occur close to this level. Above this, a pattern of waves of roughly constant amplitude tilts upstream with height.

We now compare the model vertical velocity with that derived from the aircraft and sondes *along their respective paths within the model* (e.g. Shutts, 1992). Figs. 21 (a) shows the model *versus* aircraft-derived vertical velocity along Run 2 at a height of 3.69 Km . The agreement is very good and clearly demonstrates that the model is capable of reproducing the correct wave response, in spite of its near-resonant nature and the complexity of the underlying terrain.

A similar comparison for sonde A (Fig. 21 (b)) shows good agreement in the lower troposphere at short range but phase errors become apparent at higher levels.

For this case the domain averaged resultant wave drag and net surface frictional drag vectors were computed to be (0.24, 0.26) Nm^{-2} and (0.70, 1.50) Nm^{-2} respectively. Again the size of the drag is fairly typical from the viewpoint of wave drag parametrization in numerical models, yet the domain-averaged frictional stress is significantly larger. Further details of this study can be found in Shutts and Broad (1992).

5. DISCUSSION AND CONCLUSIONS

The practical motivation for this work comes from the need to correctly parametrize gravity wave drag in numerical weather prediction and climate models (e.g. Palmer et al, 1986). The good agreement between simulated and observed vertical velocity suggests that we should have faith in the vertical momentum fluxes and form drag computed yet some caution is still appropriate. The vertical momentum flux depends critically on the ability of the model to resolve the vertical structure of the wave in regions of large Scorer parameter; to represent any wave breaking that should occur, and to provide a physically appropriate upper boundary condition. On this last point one should recall that the use of a damping layer is only appropriate if downward reflection of wave energy from above the height of the model top is unlikely. In simulations of real cases it is difficult to be certain that this will not occur and one is forced to assume that waves are very effectively dissipated at some height below any potentially reflecting layers.

The climatological fact that wind speed tends to increase with height, and static stability tends to decrease with height in the mid-latitude troposphere causes the Scorer parameter to be small in the upper troposphere - thereby favouring trapped lee waves. The majority of field experiment days with strong surface winds fell into this category, being associated with strong baroclinicity and the presence of an upper tropospheric jetstream. Some gravity wave drag parametrization schemes however, do not explicitly recognize this fact and effectively only consider horizontal wavelengths long enough for trapping to be weak.

A related question that arises is, 'Where are trapped lee waves dissipated ? for it is in these regions that the drag force will be felt. Shallow trapped lee waves may be eroded by boundary layer dissipation as they spread downstream : deep, long wavelength waves may 'leak' their disturbance energy into the stratosphere where it propagates upward and finally leads to wavebreaking through the density-induced whiplash effect. The degree of energy leakage would be an important factor in determining the height of wavebreaking since a long wavetrain with strong trapping and small upward energy flux will require more density-induced wave amplification than a more energetic disturbance coupled to a short wavetrain. It is possible that turbulence within the lee wave itself may cause downstream decay. In this case wave drag would

be experienced by the airstream in the troposphere.

In all of the model simulations described here the vertical momentum flux decreased rapidly with height in the lowest couple of kilometres and then exhibited a linear decrease with height above. The dissipation mechanism in the model is presumably horizontal diffusion : it is not clear therefore to what extent the momentum flux profiles are correct. It has to be admitted that in spite of the good verification of model vertical velocity *versus* sonde and aircraft observations we still cannot be sure that the model can give accurate information on vertical momentum fluxes needed for parametrization schemes. It would be interesting to see the same cases run on other non-hydrostatic primitive equation models.

One imagines that it is important to ensure that the model boundary layer evolves realistically over the mountains in order to achieve the correct lee wave forcing. In line with the observations of Grant and Mason (1990), we chose to implement reasonably large values of roughness length in the boundary layer scheme though in a rather arbitrary manner (linear dependence on terrain height). With gridlengths of 1 Km or greater, the distinction between wave drag and aerodynamic form drag (associated with boundary layer turbulence) is probably sufficiently clear cut that there is little 'double counting' of the latter through parametrization *and* explicit representation. Indeed, the steadiness of the flow in the boundary layer suggests that we have not transgressed into the realm of Large Eddy modelling. Yet if the horizontal resolution was increased further so that the gridlength was 250 m, the choice of a suitable z_0 would be even more difficult. The prospect of being able to numerically simulate the structure of stable boundary layers as they pass over complex hilly terrain is an exciting one and is likely to be an important adjunct to the theory of lee waves.

If the large roughness lengths chosen here are appropriate, as there is every reason to believe, it suggests that aerodynamic pressure drag and shearing stress (jointly called 'boundary layer friction') are more important than gravity wave drag in the atmosphere-to-earth momentum exchange. It is an open question as to how general a result this is. To some extent, parametrizations of gravity wave drag in numerical weather prediction models may have been compensating for deficiences in boundary layer drag parametrization over rugged terrain. Even so, the fact remains that the size of modelled gravity wave stresses is sufficiently large to imply an important effect in the momentum budget of the atmosphere.

The close agreement between model simulated vertical velocity and observed has a greater significance than proving the veracity of the model alone : it reinforces our confidence in the observing techniques themselves. Whilst it is widely recognised that the balloon rate-of-ascent technique for measuring vertical velocity is likely to be accurate, it is always possible that some of the ascent rate fluctuations are due to changes in the aerodynamic characteristics of the balloon. The favourable agreement between model and observations is therefore reassuring on more than one count.

In all, a total of five case studies have been carried out with the model in its current optimized state - three of which are the ones featured here. The wave characteristics were rather different in the other two cases; one having nearly hydrostatic waves generated in the lee of the Cumbrian mountains (Nov. 23 1991); the other taken from the Scottish field experiment (Oct. 25 1990) having highly trapped lee waves. The model/sonde comparisons in these cases were somewhat less good with some phase error. Upstream effects outside of the model domain could account for the phase errors in the highly trapped case.

Looking to the future one could imagine high resolution models such as the one used here being run on workstations for local aviation forecasting at outstations. Forecasters currently employ crude empirical methods to predict the maximum lee wave amplitude and its height of occurrence. Using orographic height data in a region local to their outstation, forecasters could routinely run a model initialized with sonde or forecast profile data and produce a relatively accurate picture of lee wave activity. From a research perspective there is a need for improved understanding of the dissipative processes responsible for lee wave decay and drag deposition. Major field experiments such as PYREX will play a central rôle in answering such questions.

Nevertheless, as shown here, small field experiments using radiosondes have a useful part to play and at relatively low cost.

6. ACKNOWLEDGMENTS

We thank Dr. P. Hignett for supplying radiosonde data during the Scottish field experiment. Dr. Stephen Mobbs, Peter Healey and Andy Macallan played a key rôle in Welsh and Cumbrian field experiments and we thank them for their contributions. We are grateful to Dr. P. Mason and A. Grant for advice concerning boundary layer roughness lengths.

References

Boer, G.J., McFarlane, N.A., Laprise,R. Henderson, J.D. and Blanchet, J.-P. (1984) The Canadian Climate Centre spectral atmospheric general circulation model. *Atmos. - Ocean.* **22**, 397-429.

Brown, P.R.A. (1983) Aircraft measurements of mountain waves and their associated flux over the British Isles. *Quart. J. Roy. Met. Soc.*, **109**, 849-866.

Carpenter, K.M. (1979) An experimental forecast using a non-hydrostatic mesoscale model. *Quart. J. Roy. Met. Soc.*, **105**, 629-655.

Corby, G.A. (1957) A preliminary study of atmospheric waves using radiosonde data. *Quart. J. Roy. Met. Soc.*, **83**, 49-60.

Durran, D.R. and Klemp, J.B. (1982) The effects of moisture on trapped lee waves. *J. Atmos. Sci.*, **39**, 2490-2506.

Golding, B.W. (1987) Short range forecasting over the United Kingdom using a mesoscale forecasting system. *Short and Medium-range Numerical Weather Prediction*, Met. Soc. Japan.

Grant, A.L.M. and Mason, P.J. (1990) Observations of boundary layer structure over complex terrain. *Quart. J. Roy. Met. Soc.*, **116**, 159-186.

Kitchen, M. and Shutts, G.J. (1990) Radiosonde observations of large amplitude gravity waves in the lower and middle stratosphere. *J. Geophys. Res.*, **95**, 20451-20455.

McFarlane, N.A. (1987) The effect of orographically excited gravity wave drag on the general circulation of the lower stratosphere and troposphere. *J. Atmos. Sci.*, 44, 1775-1800.

Palmer, T.N., Shutts, G.J. and Swinbank, R. (1986) Alleviation of a systematic westerly bias in general circulation and numerical weather prediction models through an orographic gravity wave drag parametrization. *Quart. J. Roy. Met. Soc.*, **112**, 1001-1039.

Shutts, G.J. (1992) Observations and numerical model simulation of a partially-trapped lee wave over the Welsh mountains. *Mon. Wea. Rev.*, **120**, 2056-2066.

Shutts, G.J., Mobbs, S., Healey, P. and Vosper, S. (1992) A multiple sounding technique for the study of gravity waves. *to be submitted*

Shutts, G.J. and Broad, A.S. (1992) A case study of lee waves over the Lake District, Northern England. *submitted to Quart. J. Roy. Met. Soc..*

Tapp, M.C. and White, P.W. (1976) A non-hydrostatic mesoscale model. *Quart. J. Roy. Met. Soc.*, **102**, 277-296.